CHANG CHEN
SHIQIANG SONG
QIXIN ZHANG
SHIFU ZHANG
ZHI HAN
JIANTING ZHOU
and
LIGANG ZOU

Numerical research on flow characteristics of leaking liquid in interstitial space of double-wall oil tank

The SF double-wall oil tank has an interstitial space with the thickness of 0.1 ~ 0.2 mm between the steel inner tank and FRP outer tank, and is equipped with a leak detection device to monitor the interstitial space for 24 hours. If internal structure of the interstitial space is designed unreasonably, the leaking liquid will be difficult to flow to the bottom of interstitial space, so that the leakage detection device cannot detect the leaking problem in time, leading to security risks during the operation process of double-wall oil tank. In this paper, the volume of fluid (VOF) model and the PISO algorithm are used to study the flow characteristics of the leaking liquid in interstitial space of double-wall oil tank based on FLUENT software. In order to reduce the computational complexity, the structure of the interstitial space of the SF double tank is simplified reasonably. It is believed that this research is valuable for the optimal design of the interstitial space structure of double-wall oil tank.

Keywords: *Numerical simulation, flow characteristic, leaking liquid, interstitial space, double-wall oil tank.*

1. Introduction

The SF double-wall oil tank has an interstitial space with the thickness of 0.1 ~ 0.2 mm between the inner tank and outer tank, and is equipped with a leak detection device to monitor the interstitial space for 24 hours. Once the inside tank or outside tank leaks, the sensor of the leak detection device will alarm when the bottom level of leaking liquid reaching 24 mm, thus ensuring the safe use of the double-wall oil tank. At present, the scale larger than 1 mm is generally called macro scale, and the scale of 1 m ~ 1 mm is called microscopic scale (Ran, et al., 2001). Since the gap between the inner tank and outer tank of the double-wall oil tank is only 0.1 to 0.2 mm, the flow of the leaking fluid is the micro-scale flow. The fluid is mainly affected by volume force and surface force in the course of flow (Ying, et al., 2008). With the scale reduced to the micro-scale level, the liquid surface force is increased to the dominate influence factor while it is often neglected in macroscopic flow (Lei, 2007). If the internal structure of the interstitial space is unreasonable, the leaking liquid will be difficult to flow to the bottom space between the inner tank and the outer tank, so that the leakage detection device cannot detect the leaking problem in time, leading to security risks during the operation process of double-wall oil tank.

Many scholars have studied this aspect. Glasgow, I. K described a method for bonding polyimide layers to previously patterned polyimide layers and the results of a factorial study on bond quality (Glasgow, et al., 1999). Jackman, R. J described a method for fabricating microfluidic devices in a photodefinable epoxy (SU-8) (Jackman, et al., 2001). Kelly, R. T demonstrated a new method for thermally bonding poly(methyl methacrylate) (PMMA) substrates to form microfluidic systems (Kelly and Woolley, 2003). Schlautmann, S presented a method for the bonding of a microfluidic device at room temperature, and developed a stamping process which allows the selective application of a thin glue layer to avoid filling the fluidic channels with the glue (Schlautmann, et al., 2003). Lu, C. M described an interstitial bonding technique for packaging of microfluidic chips (Lu, et al., 2008). Gu, P reported a method to bond COC with PDMS through surface activation by corona discharge, surface modification using 3-(trimethoxysilyl) propyl methacrylate (TMSPMA), and thermal annealing (Gu, et al., 2011). Kalkandjiev, K investigated TMMF photopolymer as a cost-efficient alternative to glass for the leak-tight sealing of high-density silicon microchannels (Kalkandjiev, et al., 2011).

Messrs. Chang Chen, Qixin Zhang, Associate Professor, Oil Department and Shifu Zhang, Professor, National Engineering Research Center for Disaster & Emergency Relief Equipment, Army Logistics University of PLA, Chongqing 401 331, Shiqiang Song, Master Degree, Logistics Training Center of PLA Rocket Force, Hebei 075 000, Zhi Han, Master Degree, Oil Representative Office of PLA, Beijing 100 081, Jianting Zhou, Master Degree, Assistant Engineer, Air Force Research Institute, Beijing 100 076, Ligang Zou, Weihai Yihe Specialty Equipment Mfg. Co. Ltd., Shangdong China. *Corresponding author Mr. Chang Chen, e-mail: 408430734@qq.com

Chee, P. S shown a low-cost rapid hot embossing poly (methylmeth acrylate) (PMMA)-based micropump replication with printed circuit board (PCB) mold (Chee, et al., 2013). Jiang, X presented the development of a laser microwelding method for assembly and packaging of polymer based microfluidic devices (Jiang, et al., 2015). Chen, P. C presented a novel bonding method for the assembly of thermoplastic microfluidic chips, with the aim of preventing the flow of UV adhesive into microchannels during the bonding process (Chen, et al., 2016). Wang, Z. F reviewed the major fabrication technologies for making polymer, especially thermoplastic microfluidic chips, such as micro tooling, injection molding, bonding and surface treatment, and also summarized the key challenges in fulfilling the needs of next generation microfluidic products (Wang, 2016).

It must also be mentioned that much work so far has concentrated on the field of sensor and circuit board manufacturing. Little is known, however, about studying the flow characteristics of the leaking liquid in interstitial space of double-wall oil tank based on numerical simulation method. And we demonstrate through an extensive literature review that the existing research are not capable of handling the specifics of problem in this study.

This paper focus on the flow characteristics of the leaking liquid in the interstitial space after the leakage of the double-layer oil tank, which is helpful to the optimal design of the interstitial space structure. And the rest of this paper is organized as follows. Section 2 illustrates the model establishment and basic assumptions. Section 3 presents the theoretical model and algorithms. Sections 4 and 5 conduct mesh generation and boundary condition settlement. Section 6 analyses the influence of location of leakage point, leakage velocity, and spacer distance of liquid flow interfaces on liquid flow. Section 7 concludes this paper.

2. Model establishment and basic assumptions

The function of interstitial space between the inner tank and outer tank is to ensure the leaking liquid can flow to the bottom of the interstitial space wherever the tank leakage occurs. The interstitial space has two main structures (Li, 2012, (WANG and Gao, 2012): one is based on the filamentous tape. The filamentous tape was wound 360° around the outer surface of the steel inner tank, and then the polyester film was wrapped on the outer surface of the filamentary tape, so as to form a small gap space between the filamentary tape and the polyester film. The other structures are made by brushing the paint with plastic particles at a distance from the outer surface of the steel inner tank in the circumferential direction and in the vertical direction. And, the polyester film are wrapped when the paint is cured. In the structure of double-wall oil tank, the filamentous tape and plastic particles are regarded as clearance shim. In literature (WANG and Gao, 2012), it is believed that the coasted plastic particles would form a grid leakage channel. Once the inner tank leaks, the leaking liquid flows quickly to the bottom position between the inner and outer oil tank through the gap of the plastic particles in the grid leakage channel. In this paper, we discussed the effect of plastic particles on the flow state of leaking liquid in interstitial space of double-wall oil tank under micro-scale conditions. In the actual brushing process, the clearance shim will show a random distribution phenomenon. Sometimes, the shape of clearance shim would be irregular. In order to simplify the calculation complexity, it is assumed that the clearance shims are of regular size and are regularly distributed on the outer surface of the inner tank after brushing. The simplified structure of the interstitial space is shown in Fig.1.

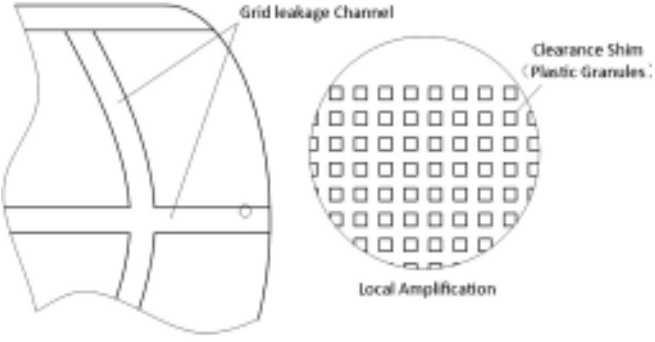

Fig.1 Simplified structure diagram of interstitial space

3. Theoretical model and algorithm

3.1 VOF MODEL

VOF (Volume of fluid) model is a surface tracking method based on fixed Eulerian grids. Two or more mutually incompatible fluid flows are simulated by solving a set of momentum equations and tracking the volume fraction of each fluid in the calculated domain (Wen, et al., 2009). This model can accurately track the free interface between the incompatible fluids by calculating the volume fraction φ_k of the k-phase flow in each control body (Ji, et al., 2011).

φ_k is listed in equation (1).

$$\phi_k(x,y,z,t)=\begin{cases}1, & \text{full filled with k-phase fluid}\\ 0, & \text{without the k-phase fluid}\\ 0\sim 1, & \text{located in the fluid interface}\end{cases} \quad ...(1)$$

For any control body, equation (2) is always established.

$$\sum_{k=1}^{n}\phi_k=1 \quad ... \quad (2)$$

In equation (2), the volume fraction φ_k can be solved by the continuity equation. That is

$$\frac{\partial}{\partial t}(\phi_k\rho_k)+\nabla\cdot(\phi_k\rho_k\mathbf{u}_k)=0 \quad ... \quad (3)$$

The momentum equations are applied to two-phase fluid that are mixed in the microchannel. The velocity field can be

obtained by solving the N-S equation based on the macroscopic continuous medium (Huang and Genxuan, 2007).

$$\frac{\partial}{\partial t}(\rho u)+\nabla\cdot(\rho uu)=-\nabla p+\nabla\cdot\left[\mu\left(\nabla u+\nabla u^{T}\right)\right]+\rho g+F \quad \ldots (4)$$

In formula (4), p represents static pressure, u represents velocity field of fluid, and u = (u, v, w), F represents the momentum source term which was produced by surface tension, ρ represents average density, μ represents kinetic viscosity. And, ρ and μ are calculated by equation (5) and (6) respectively:

$$\rho=\rho_g+\phi_l(\rho_l-\rho_g) \quad \ldots (5)$$

$$\mu=\mu_g+\phi_l(\mu_l-\mu_g) \quad \ldots (6)$$

In the above formula, the subscript g indicates gas phase, the subscript indicates liquid phase.

The continuum surface force model (CSF) was applied in the calculation of the momentum source term (Brackbill, et al., 1992):

$$F=\sigma\kappa_k\frac{\rho\nabla\phi_k}{(\rho_g+\rho_l)/2} \quad \ldots (7)$$

Segmental reconstruction method are used for the interface reconstruction and interface advancement in calculation area. The position of the interface is determined by the interface normal vector n and the volume fraction ϕ_k defined in the center of the grid, and the interface with the flow propagation is followed by the Lagrangian method. The interfacial curvature k_k is presented in formula (8):

$$\begin{cases}\kappa_k=\nabla\cdot\left(\dfrac{n}{|n|}\right)\\ n=\nabla\phi_k\end{cases} \quad \ldots (8)$$

3.2 PISO ALGORITHM

PISO (pressure implicit with splitting of operator) algorithm was proposed by Issa in 1986. The algorithm is an implicit operator splitting algorithm for solving the pressure (Issa, 1986), and its calculation process includes a prediction step and two calibration steps. In order to better satisfy the momentum equation and the continuity equation at the same time, the PISO algorithm performs two corrections for (u_x, u_y, p), which greatly improves the convergence speed of the single iteration step, but also puts forward the higher requirement of the computer's storage space. However, compared to SIMPLE algorithm, the overall efficiency of PISO algorithm is still greatly improved, especially for transient problems, the advantage of PISO algorithm is very obvious. The PISO algorithm is calculated as follows:

(1) The prediction step

Given the initial pressure field p^*, the momentum discrete equation (9) and equation (10) are solved to obtain the velocity field :

$$a_{i,J}u_{xi,J}=\sum a_{nb}u_{xnb}+(p_{I-1,J}-p_{I,J})A_{i,J}+b_{i,J} \quad \ldots (9)$$

$$a_{I,j}u_{yI,j}=\sum a_{nb}u_{ynb}+(p_{I,J-1}-p_{I,J})A_{I,j}+b_{I,j} \quad \ldots (10)$$

In equation (9) and equation (10), A represents the interface area of control volume, b represents the source term of the momentum equation.

(2) The first calibration step

The velocity field (u^*_x, u^*_y) obtained in the prediction step is generally unable to satisfy the continuity equation and must be corrected. Given a new velocity field (u^{**}_x, u^{**}_y) which satisfy the continuity equation:

$$p^{**}=p^*+p' \quad \ldots (11)$$

$$u_x^{**}=u_x^*+u_x' \quad \ldots (12)$$

$$u_y^{**}=u_y^*+u_y' \quad \ldots (13)$$

This set of formulas is used to define the corrected velocity field:

$$u^{**}_{xi,J}=u^*_{xi,J}+d_{i,J}(p'_{I-1,J}-p'_{I,J}) \quad \ldots (14)$$

$$u^{**}_{yI,j}=u^*_{yI,j}+d_{I,j}(p'_{I,J-1}-p'_{I,J}) \quad \ldots (15)$$

For the standard volume of the control body, the continuity discrete equation is:

$$\left[(\rho u_xA)_{i+1,J}-(\rho u_xA)_{i,J}\right]+\left[(\rho u_yA)_{I,J+1}-(\rho u_yA)_{I,j}\right]=0 \quad \ldots (16)$$

Substituting equations (14) and equations (15) into the continuity equation (16), the result can be obtained as follow:

$$\left\{\rho_{i+1,J}A_{i+1,J}\left[u^*_{xi+1,J}+d_{xi+1,J}(p'_{I,J}-p'_{I+1,J})\right]-\rho_{i,J}A_{i,J}\left[u^*_{xi,J}+d_{xi,J}(p'_{I-1,J}-p'_{I,J})\right]\right\}+$$
$$\left\{\rho_{I,j+1}A_{I,j+1}\left[u^*_{yI,J+1}+d_{I,j+1}(p'_{I,J}-p'_{I,J+1})\right]-\rho_{I,j}A_{I,j}\left[u^*_{yI,j}+d_{I,j}(p'_{I,J-1}-p'_{I,J})\right]\right\}=0 \quad \ldots (17)$$

Equation (17) can be abbreviated as:

$$a_{I,J}p'_{I,J}=a_{I+1,J}p'_{I+1,J}+a_{I-1,J}p'_{I-1,J}+a_{I,J+1}p'_{I,J+1}+a_{I,J-1}p'_{I,J-1}+b'_{I,J} \quad \ldots (18)$$

In equation (18),

$$\begin{cases}a_{I+1,J}=(\rho dA)_{i+1,J}\\ a_{I-1,J}=(\rho dA)_{iJ}\\ a_{I,J+1}=(\rho dA)_{Ij+1}\\ a_{I,J-1}=(\rho dA)_{Ij}\\ a_{I,J}=a_{I+1,J}+a_{I-1,J}+a_{I,J+1}+a_{I,J-1}\\ b_{I,J}=(\rho u^*_xA)_{i,J}-(\rho u^*_xA)_{i+1,J}+(\rho u^*_yA)_{I,j}-(\rho u^*_yA)_{I,j+1}\end{cases} \quad \ldots (19)$$

The first pressure correction value p' can be obtained by solving the equation (18). What is more, the velocity field ($u_x^{**}+u_y^{**}$) can be acquired by substituting the pressure correction value p' into equation (14) and equation (15).

(3) The second calibration step

The momentum discrete equation of u_x^{**} and u_y^{**} are shown as follows:

$$a_{i,J}u^{**}_{xi,J} = \sum a_{nb}u^{*}_{xnb} + \left(p^{**}_{I-1,J} - p^{**}_{I,J}\right)A_{i,J} + b_{i,J} \quad \ldots (20)$$

$$a_{I,j}u^{**}_{yI,j} = \sum a_{nb}u^{*}_{ynb} + \left(p^{**}_{I,J-1} - p^{**}_{I,J}\right)A_{I,j} + b_{I,j} \quad \ldots (21)$$

The momentum equation is solved again, and the velocity field which is corrected twice can be obtained:

$$a_{i,J}u^{***}_{xi,J} = \sum a_{nb}u^{**}_{xnb} + \left(p^{***}_{I-1,J} - p^{***}_{I,J}\right)A_{i,J} + b_{i,J} \quad \ldots (22)$$

$$a_{I,j}u^{***}_{yI,j} = \sum a_{nb}u^{**}_{ynb} + \left(p^{***}_{I,J-1} - p^{***}_{I,J}\right)A_{I,j} + b_{I,j} \quad \ldots (23)$$

To subtract equation (20) from equation (22), and subtract equation (21) from equation (23), it can be derived that:

$$u^{***}_{xi,J} = u^{**}_{xi,J} + \frac{\sum a_{nb}\left(u^{**}_{xnb} - u^{*}_{xnb}\right)}{a_{i,}} + d_{i,J}\left(p^{''}_{I-1,J} - p^{''}_{I,J}\right) \quad \ldots (24)$$

$$u^{***}_{yI,j} = u^{**}_{yI,j} + \frac{\sum a_{nb}\left(u^{**}_{ynb} - u^{*}_{ynb}\right)}{a_{Ij}} + d_{I,j}\left(p^{''}_{I,J-1} - p^{''}_{I,J}\right) \quad \ldots (25)$$

In above formula, p'' is the secondary correction of the pressure, p^{***} and can be expressed as:

$$p^{***} = p^{**} + p'' \quad \ldots (26)$$

Substituting the formula (24) and formula (25) into the continuity equation (16), the two pressure correction equation is obtained as follows:

$$a_{I,J}p^{''}_{I,J} = a_{I+1,J}p^{''}_{I+1,J} + a_{I-1,J}p^{''}_{I-1,J} + a_{I,J+1}p^{''}_{I,J+1} + a_{I,J-1}p^{''}_{I,J-1} + b^{''}_{I,J} \quad \ldots (27)$$

In equation (27),

$$\begin{cases} a_{I+1,} = \left(\rho dA\right)_{i+1,} \\ a_{I-1,} = \left(\rho dA\right)_{iJ} \\ a_{IJ1+} = \left(\rho dA\right)_{iJ1+} \\ a_{IJ1-} = \left(\rho dA\right)_{Ij} \\ a_{I,J} = a_{I+1,J} + a_{I-1,J} + a_{I,J+1} + a_{I,J-1} \\ b^{''}_{I,J} = \left(\dfrac{\rho A}{a}\right)_{i,J}\sum a_{nb}\left(u^{**}_{xnb} - u^{*}_{xnb}\right) - \left(\dfrac{\rho A}{a}\right)_{i+1,J}\sum a_{nb}\left(u^{**}_{xnb} - u^{*}_{xnb}\right) \\ \quad + \left(\dfrac{\rho A}{a}\right)_{I,j}\sum a_{nb}\left(u^{**}_{ynb} - u^{*}_{ynb}\right) - \left(\dfrac{\rho A}{a}\right)_{I,j+1}\sum a_{nb}\left(u^{**}_{ynb} - u^{*}_{ynb}\right) \end{cases} \quad \ldots (28)$$

The equation (27) is solved to obtain a secondary pressure correction value p'', so as to obtain the secondary corrected pressure field p^{***}.

$$p^{***} = p^{**} + p'' = p^{**} + p' + p'' \quad \ldots (29)$$

Finally, the second corrected velocity field can be obtained by solved equation (24) and equation (25). For the transient problem, if the calculation process is non-iterative, then it can be considered that the secondary corrected pressure field p^{***} and velocity field $\left(u^{***}_{xi}, u^{***}_{yI,j}\right)$ are accurate. The iterative calculation procedure of the steady-state flow in the PISO algorithm is shown in Fig.2.

4. Mesh generation

An example of a leak occurs in the upper part of inner oil tank

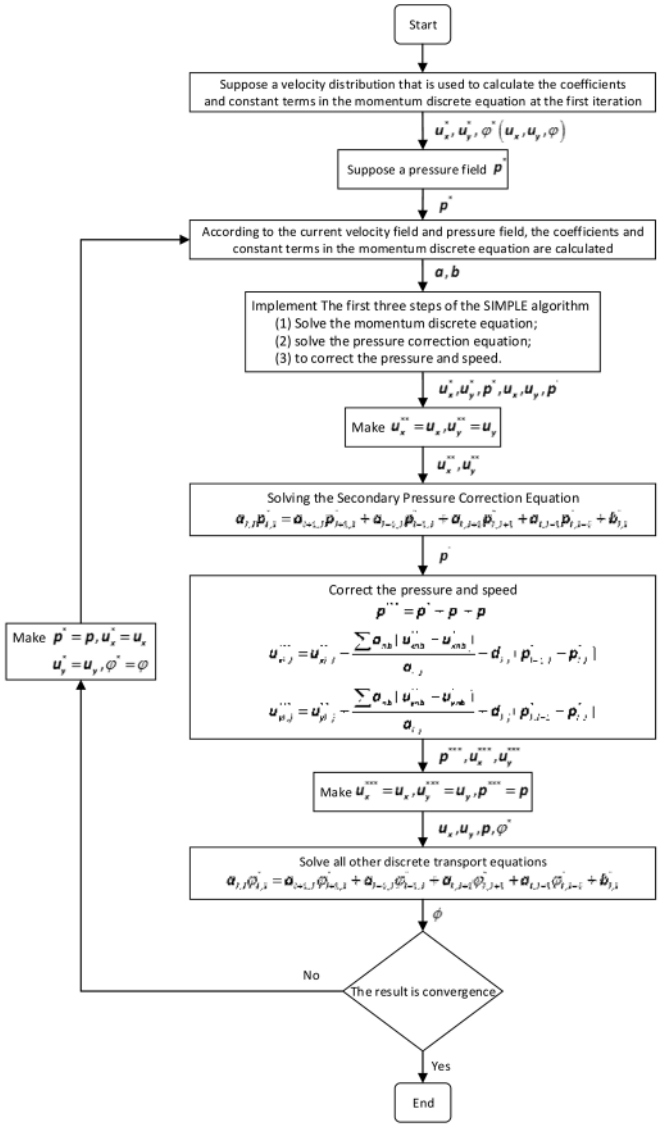

Fig.2 Flow diagram of PISO algorithm

with an interstitial space thickness of 0.2 mm is studied. The space of 5 mm×6 mm×0.2 mm near the leakage point is selected as the calculation area, and the leakage point is a circular micropore with a diameter of 0.15 mm, and the clearance shim is a regular hexahedron particle with a length of 0.2 mm and is uniformly distributed. In this paper, we mainly focus on the effect of clearance shim on the flow state of leaking liquid in interstitial space, therefore, four different relative positions are selected between the leakage point and the clearance shim. The geometric model is established by using SolidWorks software, and then the geometric model is introduced into the pre-processing software Gambit for meshing procedure. As the geometric model is relatively simple, and in order to improve the accuracy of the calculation, the hexahedral element is selected as the grid unit. The simulation calculation area and grid meshing are shown in Fig.3.

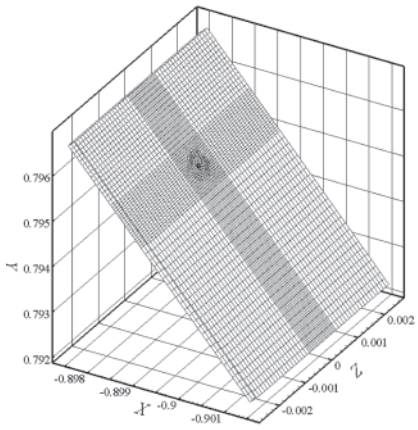

(a) No Clearance shim near the leakage point

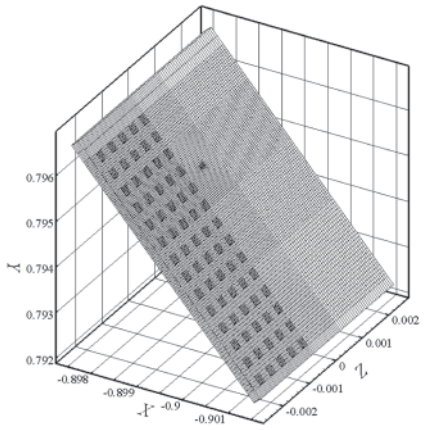

(b) Leakage point is on the outside edge of leakage channel

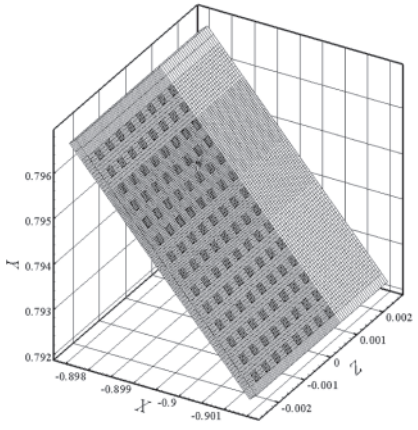

(c) Leakage point is on the inside edge of leakage channel

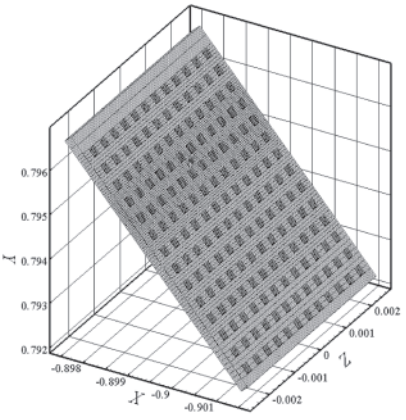

(d) Leakage point is in the leakage channel

Fig.3 Mesh grids of computation domains of different leakage sites (unit: m)

5. Bounddary condition setting

The calculation medium is the diesel and air under the standard condition, and the whole calculation process takes the influence of gravity into account. The circular micro hole of the leakage point is set as the velocity inlet boundary condition, and the area around the leakage point is set as the pressure outlet boundary condition. The working pressure keeps 101.325 Pa, and the static contact angle of the wall is 90 degrees. What is more, the wall has no slip condition. The PISO algorithm is applied to the coupling of pressure and velocity because this algorithm is better for transient simulation. In order to accelerate the convergence, the relaxation factor is set to 1. The momentum, turbulent kinetic energy, and turbulence dissipation rate are used in the second order upwind discrete format, and the initial state for the entire computing space was filled with air. The numerical simulation is carried out by using fluid calculation software Fluent, and the calculation conditions are shown in Table 1.

6 Results and analysis

6.1 Influence of location of leakage point on liquid flow

Fig.4(a) shows the liquid flow interface under the circumstance that without clearance shim near the leakage point. It can be seen from the figure that the liquid does not flow in the direction of gravity effect after it flows out of the leak point, but fills the whole gap and spreads around the leak point as the center. The diffusion distance from each direction is substantially equal. It can be inferred that the effect of the fluid force (here, gravity) on the liquid flow is almost negligible, and the liquid surface force plays a dominant role in the liquid flow.

Fig.4(b) shows the liquid flow interface under the circumstance that the leakage point is on the outside edge of leakage channel. It can be seen from the diagram that the liquid does not flow into the leakage channel, but is blocked at the boundary of the leakage channel, and in other words, the leakage passage does not play the role of guiding the flow of liquid. Due to the existence of clearance shim in leakage channel, the interstitial space is divided into a number of tiny rectangular channels. Although the leaking liquid is easy to enter the channel under the self-priming effect of those small rectangular channel when the liquid is getting closer, but the liquid stays at the microtubule exit under the influence of microtubule exit effect (Liu, et al., 2006). This is because the resistance of the liquid to the interstitial space that without clearance shim is less than the outlet resistance of the microtubules.

Table 1: Computing conditions

Leakage point location	Leakage velocity v/m·s^{-1}	Separation distance between clearance shim d/mm
a, b, c, d	2	0.2
b	2, 3, 4	0.2
b	2	0.5, 0.6, 0.7, 0.8

Note: Leakage point location a, b, c, d are shown in Fig.3

Fig.4(c) shows the liquid flow interface under the circumstance that the leakage point is on the inside edge of leakage channel. It can be seen from the figure that the flow rate of leaking liquid flow out of the leakage channel is significantly larger than that in the leakage channel, which further shows that the leakage channel did not play its proper role of diversion. The main reason for this phenomenon is

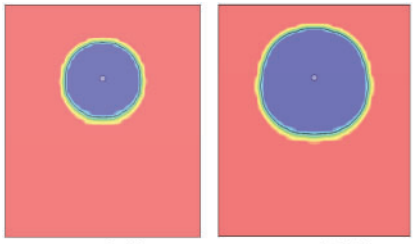

(a) Without clearance shim near the leakage point

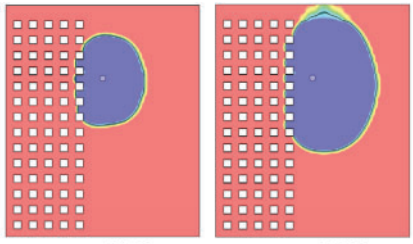

(b) Leakage point is on the outside edge of leakage channel

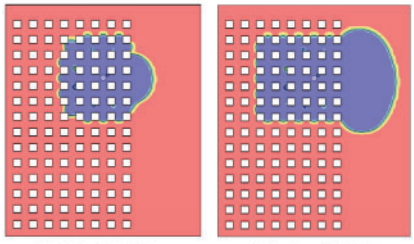

(c) Leakage point is on the inside edge of leakage channel

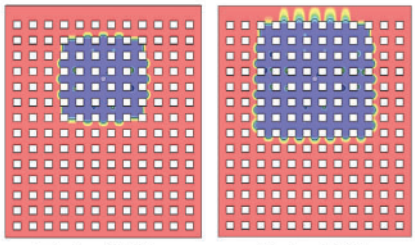

(d) Leakage point is in the leakage channel

Fig.4 Flow interfaces of liquids at different leakage sites

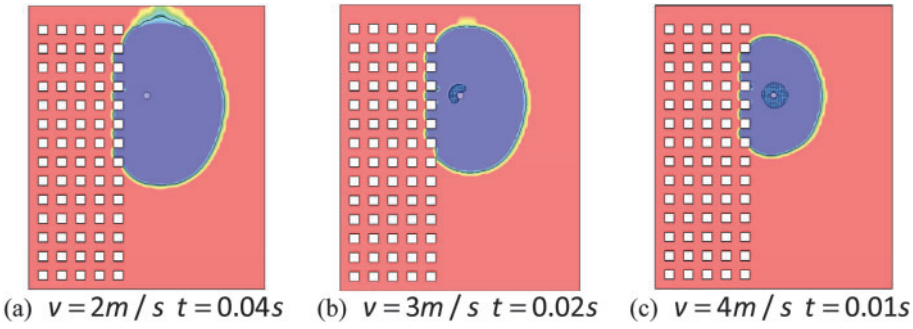

Fig.5 Flow interfaces of liquids at different leakage velocities

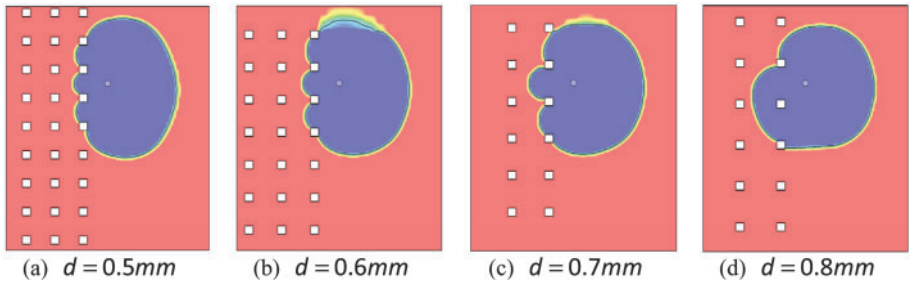

Fig.6 Liquid flow interfaces with different spacer distances at t = 0.04s

that the leaking liquid in the channel will meet microtubule outlet for every short distance movement which will impede fluid flow.

Fig.4(d) shows the liquid flow interface under the circumstance that the leakage point is in the leakage channel. In contrast to the situation in Fig.4(a), the liquid is rectangularly diffused at the point of leakage, and this is related to the distribution of the clearance shim. Due to the clearance shim between the spaces evenly distributed interstitial space into many small rectangular channels, and in the micro scale flow, influence of volume force on liquid flow is negligible, so the flow of the liquid has rectangular distribution.

In summary, it can be seen that the leakage channel of the double-wall oil tank does not actually function to direct the liquid to the bottom of the interstitial space as soon as possible, and its vertical leakage channel also prevents the leaking liquid from flowing to the bottom of the space.

6.2 Influence of leakage velocity on liquid flow

When the location or size of the leaking point changes, the leakage flow will be different. Considering the two cases, the flow characteristics of the leaking liquid with different velocity in the interstitial space are investigated. Fig.5 shows the flow interface of leaking liquids at different time when the leakage velocity are 2 m/s, 3 m/s, 4 m/s respectively. It can be seen from the figure, although the leakage rate has increased, but the flow characteristics of leaking liquid in the interstitial space did not change. And, the leaking liquid still cannot flow into the channel. What is more, as the outlet velocity increases, cavitation occurs near the leakage point.

6.3 Influence of spacer distance of liquid flow interfaces on liquid flow

Fig.6 shows the liquid flow interfaces with different spacer distances at t = 0.04s. It can be seen from the figure that when the spacer distance is less than 0.7mm, the leaking liquid cannot flow into the leakage channel. When the spacer distance reaches 0.8mm, the liquid can enter the leakage channel, but the flow velocity is obviously smaller than that in the area without clearance shim. This is mainly because when the spacer distance increases, the micro-scale effect in the vertical and horizontal directions will be weakened. When the spacer distance is reaching 0.8 mm, the scale of vertical and horizontal directions are very close to the macroscopic level. The exit resistance of the micro channel and the resistance at the non-clearance shim area have been basically

balanced, so the leaking liquid can enter the leakage channel.

7. Conclusion

In this paper, the volume of fluid (VOF) model and the PISO algorithm are used to study the flow characteristics of the leaking liquid in interstitial space of double-wall oil tank based on FLUENT software. In order to reduce the computational complexity, the structure of the interstitial space of the SF double tank is simplified reasonably. The results show that the leakage channel of the double tank cannot effectively guide the leaking liquid to the bottom of the interstitial space as soon as possible, and its vertical leakage channel will hinder the flow of the leaking liquid to the bottom of the interstitial space. The flow characteristics of the leaking liquid do not follow the change of the leakage velocity. When the spacer distance increased to 0.8 mm, the liquid side can enter the leakage channel, but its flow rate is still significantly less than that in the area without clearance shim.

Acknowledgments

This paper is supported in part by The National Key Technology R&D Program of China (2017YFC0806306), Education Science fund of the Military Science Institute of Beijing, China (No.2016JY481), and Chongqing Graduate Scientific Research Innovation Project, China (No.CYB17148).

References

1. Brackbill, J., Kothe, D. B. and Zemach, C. (1992): "A continuum method for modeling surface tension." *Journal of Computational Physics*, 100(2): 335-354.
2. Chee, P. S., Arsat, R., Hashim, U., Rahim, R. A. and Leow, P. L. (2013): "Micropump Pattern Replication Using Printed Circuit Board (PCB) Technology." *Materials and Manufacturing Processes*, 28(6): 702-706.
3. Chen, P. C., Liu, Y. M. and Chou, H. C. (2016): "An adhesive bonding method with microfabricating micro pillars to prevent clogging in a microchannel." *Journal of Micromechanics and Microengineering*, 26(4): 9.
4. Glasgow, I. K., Beebe, D. J. and White, V. E. (1999): "Design rules for polyimide solvent bonding." *Sensors and Materials*, 11(5): 269-278.
5. Gu, P., Liu, K., Chen, H., Nishida, T. and Fan, Z. H. (2011): "Chemical-Assisted Bonding of Thermoplastics/ Elastomer for Fabricating Microfluidic Valves." *Analytical Chemistry*, 83(1): 446-452.
6. Huang, D. and Genxuan, Z. (2007): "Study on the Micro Scale Flow Model." *Electro-Mechanical Engineering*, 23(3): 59-61.
7. Issa, R. I. (1986): "Solution of the implicitly discretised fluid flow equations by operator-splitting." *Journal of Computational Physics*, 62(1): 40-65.
8. Jackman, R. J., Floyd, T. M., Ghodssi, R., Schmidt, M. A. and Jensen, K. F. (2001): "Microfluidic systems with on-line UV detection fabricated in photodefinable epoxy." *Journal of Micromechanics and Microengineering*, 11(3): 263-269.
9. Ji, Z., Yudong, D., Xun, Z., Hong, W., Qiang, L. and Qiang, W. (2011): "VOF-simulation of dynamic behaviors of emerging gas bubble in mini-channel with liquid flow." *Journal of Thermal Science and Technology*, 10(2): 110-116.
10. Jiang, X., Chandrasekar, S. and Wang, C. H. (2015): "A laser microwelding method for assembly of polymer based microfluidic devices." *Optics and Lasers in Engineering*, 6698-104.
11. Kalkandjiev, K., Riegger, L., Kosse, D., Welsche, M., Gutzweiler, L., Zengerle, R. and Koltay, P. (2011): "Microfluidics in silicon/polymer technology as a cost-efficient alternative to silicon/glass." *Journal of Micromechanics and Microengineering*, 21(2): 8.
12. Kelly, R. T. and Woolley, A. T. (2003): "Thermal bonding of polymeric capillary electrophoresis microdevices in water." *Analytical Chemistry*, 75(8): 1941-1945.
13. Lei, H. (2007): "Features and affecting factors of micro size liquid movement." *Shanxi Architecture*, 33(32): 195-196.
14. Li, C. (2012): Buried double deck storage tank: China, 201120192198 [P]. 2012-02-15.
15. Liu, Z., Hou, J. and Yue, X. (2006): "Interfacial phenomena inmicro scale flowing and its flowing boundary condition." *Journal of Hydrodynamics*, 21(3): 339-346.
16. Lu, C. M., Lee, L. J. and Juang, Y. J. (2008): "Packaging of microfluidic chips via interstitial bonding." *Electrophoresis*, 29(7): 1407-1414.
17. Ran, T., Xiaobo, Q. and Jianzhong, X. (2001): "Several questions in research of micro." *Journal of Engineering Thermophysics*, 22(5): 575-577.
18. Schlautmann, S., Besselink, G. A. J., Prabhu, R. and Schasfoort, R. B. M. (2003): "Fabrication of a microfluidic chip by UV bonding at room temperature for integration of temperature-sensitive layers." *Journal of Micromechanics and Microengineering*, 13(4): S81-S84.
19. Wang, W. and Gao, D. (2012): Double layer oil storage tank and manufacturing method: China, 201210190033.8 [P]. 2012-9-26.
20. Wang, Z. F. (2016): "Fabrication Techniques for Production of Thermoplastic-Based Microfluidics Devices." *Journal of Molecular and Engineering Materials*, 4(3): 13.
21. Wen, Z., Shi, L. and Ren, Y. (2009): FLUENT computational fluid applications [M]. BeiJing:Tsinghua University Press, 2009.
22. Ying, Z., Wei, W., Li, T., Xiaowei, L. and Ling, L. (2008): "Scaling Effect of Micro Fluidic Systems." *Micronanoelectronic Technology*, 45(1): 33-37.